Physiological and transcriptional response of the diatom *Corethron hystrix* under robust UVR irradiation

Robert W. Read[1], David C. Vuono[1], Iva Neveux[1], Carl Staub[2] and Joseph J. Grzymski[1]

1. Division of Earth and Ecosystem Sciences, Desert Research Institute, Reno, NV 89512, USA

2. Agtron, Inc. 9395 Double R Blvd, Reno, NV 89521, USA

Correspondence: Joseph J. Grzymski, Department of Earth and Ecosystem Sciences, Desert Research Institute, 2215 Raggio Parkway, Reno, NV 89509, USA.

***E-mail: joeg@dri.edu**

Abstract:

A novel close-coupled and wavelength-configurable platform was designed that allows the precise and repeatable in-vitro irradiation of target organisms to determine their metabolic, protective, mutative, and repair mechanisms as a function of varying levels of specific electromagnetic energy. This new platform and an associated method to quantify near real-time electromagnetic induced stress progression in photoautotrophic organisms, provided a methodology to alter the physiological and metabolic functions of cells in a highly controlled manner. *Corethron hystrix* was selected as the target for an in-vitro UVR irradiation period of 6-hours followed by a shielded dark period of 6-hours. Irradiation and dark periods were repeated with energy levels beginning at 0.32 mW/cm^2 and increasing incrementally to 1.59 mW/cm^2. By subjecting the organism to UV induced stress, and observing/recording the physiological and molecular responses at each energy level to both UV induced damage and subsequent repair, we discovered that the cells exhibited a negative linear decrease in the photosynthetic efficiency of photosystem II proportional to UV intensity, corresponding to a large increase in the turnover time of the quinones. Gene expression changes were consistent with UVR induced photosystem II damage with decreased expression of photosystem II reaction center proteins D1, CP43 and CP47. Down-stream metabolic pathways demonstrated mixed expression after UVR irradiation, with strong up-regulation after dark recovery. This ability to alter the physiological, molecular and metabolic makeup of an organism in a highly specific manner is a valuable research and discovery tool in DNA damage research.

Introduction:

Diatoms are microscopic photosynthetic algae that are ubiquitous throughout the surface waters of the oceans (Lohman 1960) and account for roughly 40% of oceanic primary production, or one-fifth of the Earth's total primary production (Falkowski and Raven 2007). Diatoms also play a vital role in the global carbon cycle through their uptake of dissolved CO_2 and subsequent carbon fixation which provides a large proportion of the base for the entire marine food web (Armbrust 2009). Given their global distribution, diatoms have adapted to survive under a variety of environmental conditions (Ligowski et al. 2012; Verde and Prisco 2012; Marchetti et al. 2012). Unfavorable conditions such as nutrient limitation (Allen et al. 2008; Dyhrman et al. 2012; Shrestha et al. 2012; Bender et al. 2014), varying light levels (Domingues et al. 2012; Herbstová et al. 2015) and UV exposure (Wu et al. 2015) are commonplace. The latter is of particular interest because of the damaging effects UV can have on photosynthesis as well as other metabolic pathways.

In phytoplankton, UV exposure can inhibit photosynthesis, based on the relative dose and dose rate (Cullen and Lesser 1991). An inhibition of the photosynthetic rate causes a decrease in the rate of primary production, with consequences in marine ecosystems as well as terrestrial environments. Phytoplankton can also produce protective compounds to combat the deleterious effects of UVR such as mycosporine-like amino acids (MAAs), DNA photolyases and many more undefined compounds (Helbling et al. 1996; Coesel et al. 2009). These compounds have shown promise in reducing the carcinogenic effects of UV irradiation, when added to commercial products such as sunscreen (Berardesca et al. 2012; Emanuele et al. 2013). Furthermore, despite the

59 tremendous diversity of diatoms, with species estimates ranging from 1×10^4 (Norton et
60 al. 1996) to 2×10^5 (Allen et al. 2006), few studies have focused on the potential
61 biomedical applications of bioactive compounds produced by these organisms (Coesel et
62 al. 2009; Prestegard et al. 2009).

63 Fluorescence kinetics measurements are a reliable estimator of photosynthetic
64 electron transport rates and photosystem II health (Kolber and Falkowski 1993) in
65 photoautotrophic organisms. Fast Repetition Rate Fluorometry (FRRF) has been used to
66 examine variations in several photosynthetic parameters in relation to light impacts on the
67 cell (Kolber et al. 1998). Changes in parameters such as the maximum quantum yield of
68 PSII (Fv/Fm) (Geider et al. 1993; Kolber and Falkowski 1993), the turnover time of
69 electron transport from QA -> QB (tau1) and QB -> PQ (tau2) (Kolber et al. 1988), and
70 the functional cross section of photosystem II (σ_{PSII}) -- the effective target size of the
71 PSII antenna in $Å^2$ $(quanta)^{-1}$ (Kolber et al. 1998), act as proxies to monitor electron
72 transport rates and the relative health of photosystem II. Here we use them to monitor the
73 speed and intensity of photosynthetic damage within the cell. Changes in these
74 parameters are a function of the dose and dosage rate of absorbed radiation, as this has a
75 direct impact of the oxidation state of PSII electron transport chain.

76 In this study, the diatom *Corethron hystrix* (CCMP 308) was subjected to
77 increasing intensities of UVR energy ranging from 0.32 mW/cm^2 to 1.59 mW/cm^2 using a
78 custom built UVR emitter array. This gave us the ability to precisely and repeatedly
79 control and measure damage as a decrease in the photochemical efficiency of PSII using
80 FRRF. Fv/Fm, sigma/σ_{PSII}, and tau were monitored hourly or bihourly to measure the
81 UV damage to PSII relative to non-irradiated conditions. Gene expression changes were

also monitored at 0.64 mW/cm^2. Our observations indicate that UV-induced damage to PSII is a linear function of time/energy irradiation. The changes in gene expression following UV irradiation and a shielded dark period of 6-hours further demonstrated that severe damage as well as preliminary repair occurred in response to UV irradiation. This study thus provides a comprehensive investigation of the physiological and molecular stress response to UV irradiation using a UV emitter array designed specifically to dose planktonic phototroph cultures with any desired UVR intensity. These tools and methods can be used to manipulate organisms that may have value in better understanding how organisms protect themselves against DNA damage.

Materials and Methods:

Cell Cultures

Corethron hystrix was grown at a maintenance temperature of 14 ºC under 12:12 L:D at an illumination of ~40 µmol photons m^{-2} s^{-1} using white LEDs. Although 14 ºC was the recommended temperature for in-vitro studies, *Corethron hystrix* has a much wider known temperature range. Duplicate cultures were grown in L1 medium (Guillard and Hargraves 1993), prepared with 0.2 µm filtered surface seawater from the Gulf of Maine (NCMA). Chlorophyll pigment extraction was accomplished in 90% acetone at -20 ºC for 17 hours, under zero light conditions. Following extraction, fluorescence of each sub-sample was measured using a 10AU Fluorometer (Turner Designs, Sunnyvale, CA, USA), and chlorophyll concentrations were calculated. Cell counts were determined using a Sedgewick chamber under bright light. Specific growth rates of replicates in the cultures were estimated from the log-linear portion of growth curves constructed from

105 chlorophyll a fluorescence and cell counts obtained under non-irradiating conditions.
106 During the UVR irradiation experiments chlorophyll a measurements and morphological
107 cell counts were also collected bihourly in order to observe how these values were
108 affected by UVR.

109 *Photosynthetic Kinetics*

110 Fv/Fm, sigma, and tau measurements were monitored using a FRRF (Soliense, Inc).
111 Cell cultures, in duplicate, were subjected to either bright white light only at ~ 40 µmol
112 m^{-2} sec^{-1} (control condition) or a combination of bright white light (~ 40 µmol m^{-2} sec^{-1})
113 and UVR irradiation ranging from 0.32 mW/cm^2 to 1.59 mW/cm^2 (experimental
114 condition). This was accomplished using a custom-built emitter platform (Lumenautix
115 Inc., Reno, NV; Fig. 1). The overall experimental period consisted of both control and
116 experimental conditions running for six hours, followed by a dark no light period of six
117 hours.

118 *NEST Configurable Emitter Array*

119 The NEST array is comprised of multiple discrete solid-state emitters operating in
120 two categories, VIS and UV connected to a control unit (Supplemental Text). The NEST
121 emitter control unit is a custom designed four-channel isolated direct current analog
122 power supply designed specifically to provide temperature stable and highly regulated
123 clean DC power to each of the four emitter channels of the NEST emitter array. The
124 output is regulated and temperature compensated for constant current DC – this allows
125 precise control and stability of light output. Voltage and current are output for power
126 adjustment and monitoring of each channel and each channel is limited to the LED output
127 safe area of operation. The NEST array consists of surface mount technology LEDs.

Visible LEDs are blue (3), red (3) and white (6) and the UV emitters (3). For this work only the UV and white LEDs were used. The white LED color temperature is 3985K and the output can vary between 4 and 380 μmol m^{-2} sec^{-1}.

The platform is close-coupled and wavelength-configurable (Fig. 1). It is designed to allow the precise and repeatable incremental in-vitro irradiation of target organisms to determine their metabolic, protective, mutative, and repair properties as a function of varying levels of specific electromagnetic energy. The platform is flexible and can be configured to emit Infrared, specific narrow-band VIS, PAR, UV, or combinations thereof. The energy categories can be adjusted incrementally and independently to affect organism behavior and biological functions, stress the organism to evoke specific physiological responses or cause DNA / RNA mutations.

Net UVR organism exposure was reported from the emitter array's gross output after subtracting attenuation from surface reflection, transmittance, absorption, and diffusion of the quartz glass container and seawater. This attenuation was approximately 25% of the gross emitter output. Data was collected every hour for UVR energy intensities of 0.32 and 0.64 mW/cm^2. At higher doses of 0.96 - 1.59 mW/cm^2, measurements were collected every 30 minutes. Raw data was processed and plotted using the ggplot2 package in the R environment (Wickham 2009). Rate constants for both Fv/Fm and sigma were calculated using a linear regression model within R.

Illumina sequencing and Gene Expression analysis

After photosynthetic kinetic measurements were made, total RNA was extracted in duplicate from cells in the mid-exponential phase of growth directly after UVR irradiation (experimental and control cultures), as well as directly after a dark recovery

period of six hours (experimental and control cultures), using the Ambion ToTALLY RNA kit (Life Technologies, Grand Island, NY, USA). The same experimental and control cultures in duplicate were used during both harvesting periods. These extractions produced approximately ~10-12 µg of total RNA from each pellet. Samples were sent for sequencing at the Biodesign Institute at Arizona State University (Tempe, AZ, USA). Library preparation was fully automated and performed using the Apollo 324 liquid handling platform. Illumina HiSeq Sequencing yielded 2x100 bp paired-end reads.

Raw sequencing reads were uploaded to the sequencing read archive (NCBI accession: SRP091884, SRX2255404) and inspected using Fastqc (Andrews 2009) to determine quality, ambiguous read percentage and relative amount of sequence reads. Illumina RNA sequencing resulted in an average of 19.4 million raw reads per cDNA library with an average quality score of Q38 (Supplementary Table S1).

Raw Sequencing reads were trimmed using the sequence trimming program Trimmomatic with the following options: Remove any Illumina adapter, cut off the end of any read where the quality score falls below 10, use a sliding window of 5 to cut and trim any base where the average quality score falls below 32 for that window and only keep trimmed reads with a minimum length of 72. (Bolger et al. 2014). De-novo transcript assembly was accomplished in Velvet (Zerbino and Birney 2008). Optimal k-mer selection, as well as read coverage cutoff selection, was determined by the VelvetOptimiser (Gladman and Seemann). Velvet-constructed contigs were assembled into full-length transcripts using the Oases transcriptome assembler, with a minimum transcript length of 150 base pairs (Schulz et al. 2012). Raw sequences were aligned to the assembled transcripts by Bowtie2 (Langmead and Salzberg 2012). Abundances of

174 mapped sequence reads were calculated using eXpress (Roberts and Pachter 2012),
175 providing the estimated count of reads that mapped to each individual assembled
176 transcript. Estimated counts from eXpress were normalized and gene expression was
177 calculated using the algorithm of DESeq2 (Love et al. 2014). Transcripts were considered
178 differentially expressed if their associated $\log_2$ fold changes were significant at a $p<0.01$,
179 based on the Wald test of DESeq24 (Love et al. 2014). Based on our experimental design,
180 differential expression was compared between the UVR+white light irradiated cells
181 (experimental treatment – in duplicate) and bright white light only cells (control
182 treatment – in duplicate), directly after the six hour UVR irradiation ended and also after
183 a six hour dark period.
184 *Corethron hystrix* is not well annotated at the current time. Therefore, to increase
185 our understanding of gene expression changes for a select set of pathways, the model
186 centric diatom *Thalassiosira pseudonana* was used as a homolog. For each pathway of
187 interest, the entire annotated pathway was downloaded from the Kyoto Encyclopedia of
188 Genes and Genomes (KEGG) (Kanehisa and Goto 2000; Kanehisa et al. 2013). *C. hystrix*
189 transcripts from our de-novo assembly were in-silica translated and compared to *T.*
190 *pseudonana* proteins using HHsearch, which is part of the HH-suite software package
191 (Remmert et al. 2012). Using hidden Markov model alignments from HHsearch allowed
192 for the discovery of any homologous proteins based on protein-protein homology (Soding
193 2005). Translated transcripts were considered homologs if there was a >90% probability
194 of the translated transcript being a homolog to the *T. pseudonana* protein. For each
195 pathway tested, translated transcripts mapping to a homolog were sometimes one of

several isoforms. To maintain consistent mapping between homologs, transcript isoforms were binned by functional annotation after translation.

In most cases, up and down regulation variation between isoforms was small, making expression patterns more evident. However, in other cases, transcript isoform variation was higher, where transcripts for the same functional annotation but different loci were both up and down regulated. Because *C. hystrix* doesn't have an annotated genome, binning by functional annotation produces an expression overview for the homolog, which accounts for transcriptional variability. Binned isoforms were visualized with a box and whisker plot using the ggplot2 package (Wickham 2009). The line in the box represents the median $\log_2$ fold change when combining all the isoforms. The hinges are the 1st and 3rd quartile.

Results:

Chlorophyll A and Cell Counts under laboratory conditions

Corethron hystrix grew at rate of 0.37 doublings per day based on chlorophyll a concentration (Fig. S1a); this was consistent with microscopic cell counts, which produced a growth rate of 0.392 doublings per day (Fig. S1b). Under UV light of different intensities, chlorophyll a content remained relatively constant during the six-hour UVR irradiation period (Fig. S2). However, light microscopy revealed morphologically altered cells in the UVR exposed cultures compared to control cultures. The percentage of morphologically intact cells was fairly constant for the lower UVR intensity levels (0.32 - 0.64 mW/cm^2), with a small decrease during the last two hours at 0.64 mW/cm^2 (Fig. S3). However, higher intensities (0.96 - 1.59 mW/cm^2) caused a

219 pronounced decrease in the amount of morphologically intact cells, especially during the
220 last two hours of UVR irradiation (Fig. S3).

221 *Photosystem II*

222 Photosynthesis is often illustrated using a simplified diagram called the Z
223 Scheme, with the first major complex being photosystem II. To monitor the changes in
224 photosystem II during exposure to UVR irradiation from a custom built UV emitter (Fig.
225 1), photosynthetic kinetic measurements were recorded for *C. hystrix* using FRRF (Fig.
226 2). There were several parameters produced by the FRRF. First, Fv/Fm measures the
227 maximum quantum yield of PSII (Fig. 2A) (Geider et al. 1993; Kolber and Falkowski
228 1993). Fv/Fm is a dimensionless parameter but represents how efficiently absorbed
229 photons are used for electron flow (Suggett et al. 2009). Higher values of Fv/Fm often
230 indicate greater efficiency and low values indicate lower efficiency. A second parameter,
231 sigma is a proxy for the functional cross section for photosystem II and is roughly
232 proportional to the PSII antenna size, or the number of chlorophyll molecules per
233 photosystem II reaction center (Fig. 2B) (Mauzerall 1986; Oxborough et al. 2012).

234 Fv/Fm decreased in a linear manner with the rate of decay increasing with
235 intensity (Supplementary Tables S2-S7). Conversely, sigma increased in a linear manner
236 with increasing intensity although at the higher intensities there was a drop in the rate as
237 photosynthesis becomes severely inhibited (Supplementary Tables S2-S7). Overall, UVR
238 had a powerful effect on the fluorescence kinetics of PSII, especially at the higher UVR
239 intensities (0.96 - 1.59 mW/cm^2, measured at 285 nm) (Fig. 2, S4-S8). For example,
240 sigma increased only 15% over the entire irradiation period at the lowest UVR intensity
241 of 0.32 mW/cm^2, with the largest increases evident after 3 hours under irradiation (Fig

S4, Supplementary Table S3). In comparison, at 0.96 mW/cm^2, we observed a similar 15% increase in sigma within the first 2 hours of UVR irradiation, with a total increase in sigma of approximately 56% over the irradiation period (Fig. S6, Supplementary Table S5). Furthermore, UVR intensities of 0.96 mW/cm^2 and 1.28 mW/cm^2 had very strong and similar responses. The rate of change of sigma for each of these two treatments was almost identical and approximately 44% faster than the rate of change observed at 0.64 mW/cm^2 (Supplementary Table S2) and 72% faster than the rate observed at 0.32 mW/cm^2. At the highest intensity of 1.59 mW/cm^2, the rate of change for sigma was slower than the rate at 0.96 mW/cm^2 and 1.28 mW/cm^2, likely because of extreme damage to the photosynthetic reaction centers. We also observe the photosynthetic efficiency at 0.64 mW/cm^2 after 4 hours is approximately the same as the as it is at 1.59 mW/cm^2 after roughly 2.5 hours. Together these results demonstrate the ability of our light engine to directly manipulate photosynthetic efficiency and target physiological states based on UVR exposure.

We also used comparative transcriptomics to evaluate the expression response of *C. hystrix* photosystem II transcripts to UV irradiation (0.64 mW/cm^2 UVR intensity). To monitor *C. hystrix* gene expression in the context of specific pathways, our reads were in-silica translated and mapped to the proteins from the ubiquitous model centric diatom *Thalassiosira pseudonana*, as the majority of its cellular pathways are at least partially annotated by KEGG (Kanehisa and Goto 2000; Kanehisa et al. 2013). There were 22 photosystem II transcripts that were differentially expressed directly after UVR irradiation (Fig. 3). Most (19/22, 86%) transcripts, after in-silica translation, mapped to photosynthetic *T. pseudonana* photosystem II homologs that demonstrated little variation

in their fold changes, indicating a strong and coordinated transcriptional response (Fig. 3, Supplementary Table S8). The majority of the photosystem II associated transcripts (20/22, 90%) were down regulated, including the reaction center core D1 protein and reaction center core antenna proteins CP43 and CP47, correlating with decreases in the photosynthetic efficiency. Moreover, in-silica translated transcripts mapping to water splitting cytochrome c550 and photosystem II PsbU proteins were also strongly down regulated.

Reoxidation of the Electron Acceptors

Tau 1 or the fast rate constant approximates the turnover time for an electron to reduce the primary quinone acceptor, QA (Falkowski and Raven 2007). Tau 2 or the slow rate constant, measures the turnover time for an electron to reduce the secondary plastoquinone acceptor, QB (Falkowski and Raven 2007). Results show that tau 1 increases as energy increases (Fig. 2C). There was very little change in tau 1 during the first 2.5 hours for any dose of UVR irradiation. After 2.5 hours, turnover time began to increase for the larger UVR doses: 0.96, 1.28, and 1.59 mW/cm^2 (Fig. 2). Overall, tau 1 turnover time increased from 26.61 µs at 0.32 mW/cm^2 to 1114.0 µs at 1.28 mW/cm^2 -- an approximately 42x increase (Supplementary Table S9). At the highest UVR energy (1.59 mW/cm^2), tau 1 turnover time initially followed the same trend as 1.28 mW/cm^2. However, there was a significant decline in the turnover time after 5 hours (Fig. 2C, Supplementary Table S9), likely because photosynthesis had become severely inhibited.

Tau 2 reacted similarly to tau 1 during UVR irradiation, although turnover time for tau 2 was much longer, on the order of seconds instead of microseconds (Fig. 2D). For the first two hours of irradiation, there was no significant change in the turnover rate

for tau 2 (Fig. 2D). After 2.5 hours, tau 2 increased with each successive increase in UVR energy, with the exception of 1.59 mW/cm^2, which decreased after 5 hours, similar to the behavior of tau 1 for the same treatment (Fig. 2D, Supplementary Table S10).

Together, tau 1 and tau 2 again demonstrate the ability of our emitter to induce certain physiological states based on set doses and dosage rates. For example, the turnover time for both tau 1 and tau 2 at 5 hours under a UVR intensity of 0.64 mW/cm^2 was the same as the turnover time for 1.28 mW/cm^2 at just 2 hours of irradiation. Also, doubling the UVR energy cut the time in half for tau 1 and 2 to reach specific turnover times -- a 1:1 ratio.

Comparative transcriptomics for the supplemental electron transport portion of the Z scheme are similar to the observations regarding photosystem II expression. There were 14 transcripts related to supplemental electron transport, most of which are a functional subunit of the cytochrome b6 complex with the "Pet" moniker. Differential expression of the 14 transcripts show 11 decreased in abundance and 3 increased, illustrating that there is a coordinated down-regulation of the supplemental electron genes. This is consistent with kinetic analysis where we see an increase in tau 1 and tau 2 turnover times for the 0.64 mW/cm^2 UVR intensity.

Photosystem I

Photosynthetic kinetic measurements for photosystem I are not reported in this study. However, gene expression measurements were conducted to see what photosystem I genes were specifically altered during UVR irradiation (Fig. 3). There were 13 photosystem I related transcripts; 12 of them decreased in abundance compared to non-irradiated samples after UVR irradiation. Included in these 12 transcripts are six variants

311 of *psaB*, a main photosystem I reaction center protein. Each one of them was strongly
312 decreased in abundance compared to the control samples.

313 *Other Metabolic Pathway Expression*

314 Fine control of the glycolytic regulation in plants is accomplished by 3 main
315 genes: hexokinase, phosphofructokinase and pyruvate kinase (Plaxton 1996). From the
316 glycolysis pathway, there were 33 differentially expressed in-silica translated transcripts
317 mapping to 12 homologous *T. pseudonana* proteins. The majority of the translated
318 transcripts mapping to homologous proteins phosphofructokinase, phosphoglycerate
319 kinase and enolase decreased in abundance directly after UVR irradiation (Fig. 4,
320 Supplementary Table S11). The hexokinase homolog did not map to any translated
321 transcript hits in our data. The expression for the rest of the glycolytic transcripts was
322 mixed with up and down regulated transcripts, however; the slight majority of transcripts
323 were increased in abundance directly after UVR irradiation.

324 The TCA cycle, the second phase of carbohydrate catabolism, is an important
325 source of the cellular reducing agent NADH, which helps generate the proton gradient
326 that is critical for the production of ATP through electron transport (Nelson and Cox
327 2005). For this pathway, we observed 47 differentially expressed in-silica translated
328 transcripts mapping to 10 homologous proteins in the TCA cycle (Supplementary Table
329 S12). The rate limiting step of the TCA cycle, Isocitrate Dehydrogenase, did not have
330 homologous proteins currently identified in *T. pseudonana*. We used Blastx against the
331 non-redundant protein database to identify a single possible Isocirate Dehydrogenase
332 transcript in our dataset, however it was not significantly differentially expressed. The
333 overall expression of the TCA cycle was mixed with approximately the same number of

334 up and down-regulated transcripts: 22 transcripts (46.8%) increased in abundance while
335 25 (53.2%) decreased (Fig. 5, Supplementary Table S12). Moreover, we observed that
336 homologs near the end of the TCA cycle, such as succinate dehydrogenase, fumarate
337 hydratase and malate dehydrogenase produced mixed expression as well (Fig. 5).
338 The Calvin-Benson-Bassham (CBB) cycle, a light independent pathway
339 necessary for CO_2 reduction, also produced mixed gene expression changes when
340 sampled after UVR irradiation (Nelson and Cox 2005) (Fig. 6, Supplementary Table
341 S13). There were homologs to 13 of 16 proteins identified in KEGG, with 95 total
342 transcript variants (Supplementary Table S13). The large subunit of RuBisCO mapped to
343 17 in-silica translated transcripts which were the isoforms of 4 gene loci (Supplementary
344 Table S13). The overall expression of the 17 RuBisCO transcripts was mixed, although
345 the majority of them were decreased in abundance (12/17 transcripts) (Fig. 6).
346 *Preliminary Recovery*
347 In contrast to the results seen directly after UVR irradiation and cellular damage,
348 transcripts in the three auxiliary metabolic pathways greatly increased in abundance after
349 dark recovery (Fig. 3-6, Supplementary Tables S14-S17). Approximately 90% of the in-
350 silica translated transcripts that mapped to homologous glycolytic, TCA and CBB cycle
351 pathway homologs increased their abundance, even after a short dark recovery period of
352 6 hours. Those transcripts produced large $\log_2$ fold changes, with several greater than $\log_2$
353 of 7. Moreover, several photosynthetic transcripts were observed to reverse their
354 expression after six hours of dark recovery.
355
356 **Discussion:**

Controlled laboratory studies describing the impact of UV on phytoplankton have the potential to improve our understanding of the photosynthetic damage and repair. To develop a controlled laboratory methodology for studying the impacts of UVR on photosynthetic and metabolic pathways, we developed a UV light emitter to deliver repeatable doses at a high resolution across a wide spectrum of intensities. As a proof of concept test of our emitter array, we selected a cosmopolitan open-ocean diatom, of which members of its genus are found in the Southern Ocean where UV intensity is high due to ozone depletion. For example, during the spring, pennate and centric diatoms comprise a large portion of the Southern Ocean biomass, and the genus *Corethron* is one of the top four genera (Vincent 1988). We chose the diatom *Corethron hystrix* for our study.

Growth Rate and Cell Morphology

The growth rate for laboratory grown *C. hystrix* under normal photosynthetically active radiation (PAR, ~40 µmol m^{-2} s^{-1}) conditions was similar to published values for several diatoms under analogous light levels (Gilstad and Sakshaug 1990). Higher level plants that can maintain chlorophyll levels during UVR irradiation may have a higher tolerance to UVR stress, as they are able to more efficiently transfer their excitation energy into photosystem II reaction center proteins (Bornman and Vogelmann 1991; Greenberg et al. 1997). During the 6 hour UVR irradiation experiment, total chlorophyll a did not change at any level of UVR irradiation. There was no significant increase in cell growth over the irradiation period. However, chloroplast morphology was altered at UVR irradiation levels of 0.64-1.59 mW/cm^2 with the largest decreases in intact chloroplasts occurring during the last two hours of irradiation. Morphological alterations consisted of

jagged chloroplasts that migrated toward the center of the cell, which could be a response similar to the "chloroplast clumping" phenomenon seen in other organisms as a form of UV protection (Sharon et al. 2011).

Photosynthetic Kinetics and Gene Expression

We used 285nm UVR irradiation (12nm FWHM; 0.32-1.59 mW/cm^2), which allowed us to manipulate the dose and rate of photosystem II damage in an approximately linear fashion by fine adjustments to the output. Photosystem II damage was affected by both intensity and time under irradiation in our study: damage from the highest UVR irradiation treatments ultimately resulted in a loss of photosynthetic function – Fv/Fm becomes approximately zero (Fig. 2A, S4-S8). There was an inverse correlation of sigma and Fv/Fm for all doses of UVR in this study, with sigma increasing and Fv/Fm decreasing as damage accumulated (Fig. 2 AB, S4-S8). The observed decrease in Fv/Fm is likely caused by UVR directly damaging photosystem II reaction centers causing a decrease in the energy transfer between its reaction center proteins. We hypothesize that the corresponding increase in sigma may be an environmental adaption to the extreme conditions. Under these conditions, chlorophyll molecules may be funneling their excitation energy away from the damaged reaction centers and into the remaining functional reaction centers, thus increasing the energy transfer of those intact reaction centers.

We observed that UVR intensity begins to have a significant effect on the photosynthetic efficiency and energy transfer by 3 hours at the 0.32 mW/cm^2 dose. At this point, it is likely that the repair system responsible for photosystem II damage has been overwhelmed and cannot keep up with the damage that is occurring to the reaction

403 centers, thus we see an increase in sigma and decrease in Fv/Fm. At higher irradiations
404 (0.96 – 1.28 mW/cm^2), the increase in energy transfer is much faster, perhaps because
405 more reaction centers are being irrevocably damaged and at a quicker pace. This leaves
406 more excitation energy for the chlorophyll molecules to pass on to the functional reaction
407 centers. We observed a noticeable decrease in sigma as the experimental period ends for
408 both 0.96 and 1.28 mW/cm^2, which possibly indicates that the majority of the reaction
409 centers have been damaged or that chlorophyll can no longer funnel their excitation
410 energy through the functional reaction centers (i.e., a loss of photosynthetic function).
411 This also may correlate to the slower increase in energy transfer at the highest irradiation
412 of 1.59 mW/cm^2 compared to 0.96 and 1.28 mW/cm^2. The damage may be so intense at
413 that irradiation that the chlorophyll molecules cannot funnel their energy into the
414 functional reaction centers as efficiently as they do at the lower irradiations. We also
415 observed that our emitter array linearly allows us to specifically set dose and dosage rate
416 to reach a certain physiological state, as evidenced by the culture irradiated at 1.59
417 mW/cm^2 reaching a photosynthetic efficiency in roughly half the time it would have
418 taken a culture irradiated at 0.64 mW/cm^2. This would allow future applications to
419 determine whether molecular changes under a fast damage rate are the same as those
420 changes under a more gradual damage rate. Moreover, at very quick damage rates, certain
421 metabolites may be produced by the cell that would not be observed at slower rates of
422 damage.

423 Low Fv/Fm measurements often signal a decrease in the efficiency of
424 photosynthesis (i.e., dynamic photoinhibition), as seen in the coccolithophorid *Emiliania*
425 *huxleyi* due to high photon flux densities (Critchley 2000; Ragni et al. 2008).

Photoinhibition is typically caused by environmental stressors such as too high or low intensities of photosynthetically active radiation (PAR), adverse temperatures, and water limitation. Our decreased Fv/Fm measurements after UVR irradiation appear to mimic photoinhibition, which is likely due to direct damage to PSII by UVR. We collected transcriptomic data after 6 hours of UVR at the intensitiy of 0.64 mW/cm^2 to explore the molecular changes undergone by the cell. As stated above photosynthetic efficiency is strongly decreased for UVR intensities of 0.64 – 1.59 mW/cm^2. Photosystem II is known to be the most sensitive part of the photosynthetic system to UVR irradiation, especially the oxygen evolving complex (Post et al. 1996; Szilárd et al. 2007). Transcriptomic analysis shows that oxygen evolving complex genes, *psbO* and *psbQ*, mapped to transcripts that decreased in abundance. *PsbO* codes for a photosystem II oxygen-evolving enhancer protein and *psbQ* codes for a photosystem II oxygen-evolving enhancer protein 3.

Furthermore, it is highly likely that there was other reaction center damage, as the D1 protein and the aromatic tyrosine electron donors were previously shown to be sensitive to UV irradiation (Vass et al. 1996; Bouchard et al. 2006). D1 is one of two main reaction center proteins, while tyrosine amino acids are part of the donor side of photosystem II absorbing energy at 285nm, thus making them a possible target for UVR irradiation (Vass et al. 1996). Transcriptome changes demonstrate that the D1 reaction center protein, encoded by the *psbA* gene, decreased in abundance during UVR irradiation compared to non-irradiated cells. It has been determined that the overall changes in the expression of *psbA* differ based on the specific organism (Surplus et al. 1998; Huang et al. 2002), however, the decrease in abundance of our *psbA* transcripts

449 during UVR was similar to the changes produced by *Arabidopsis thaliana* (Surplus et al.
450 1998). Other reaction center proteins, such as the CP47 chlorophyll apoprotein which
451 along with its sister protein CP43 channel the energy from the light harvesting complexes
452 to the reaction center core, (Falkowski and Raven 2007) also displayed large decreases in
453 abundance after UVR irradiation. Previously, it was observed that both CP47 and CP43
454 expression levels decreased in the cyanobacteria *Spirulina platensis* during UVR
455 irradiation (Rajagopal et al. 2000), and our observations were consistent with that study.
456 This result also lends credence to the hypothesis that the functional cross section of PSII
457 increases because of damage to reaction center proteins and the re-allocation of energy
458 transfer to functional centers.

459 Tau is a proxy for the turnover time for the photosystem II reaction center (Kolber
460 et al. 1988). Both tau 1 and tau 2 turnover times increase significantly at UVR
461 irradiations of 0.64-1.59 mW/cm^2 (Fig. 2CD). This is likely because the plastoquinones
462 QA and QB are directly susceptible to UVR damage (Melis et al. 1992). Our data also
463 illustrate that turnover time is inversely correlated higher intensities (Fig. S4-S8, Tables
464 S3-S7, S9 & S10). With turnover times increasing to 1 – 1.5 seconds in certain cases
465 (Fig. 2D), these long reoxidation times likely have a detrimental effect on photosynthesis,
466 thus explaining the almost complete loss of photosynthetic function at higher intensities
467 of UVR.

468 Transcriptome analysis of supplemental photosynthetic electron transport genes
469 corresponds with our photosystem II expression analysis, as the majority of the
470 transcripts were down-regulated compared to the control samples. Most of the translated
471 transcripts in this subset of data mapped to homologous cytochrome b6-f complex

472 proteins. There are 4 major subunits that make up the cytochrome b6-f complex in algae
473 (Pierre et al. 1995). We discovered in our data that both of the heme-bearing subunits of
474 the cytochrome b6-f complex were strongly down-regulated after UVR irradiation. We
475 didn't have any homologous hits to the other two cytochrome b6-f subunits, however, the
476 other supplemental photosynthetic electron genes, such as *petF* and *petH*, were also
477 decreased in abundance compared to the non-irradiated control samples.
478 The final stage of the photosynthetic light reaction is characterized by
479 photosystem I. Photosystem I isn't directly affected by UVR irradiation, and is more
480 resistant to environmental stressors such as high-light levels (Teramura and Ziska 1996;
481 Zhang et al. 2016). However, due to interaction between photosystem II and photosystem
482 I during photosynthesis, UVR irradiation will unavoidably have an effect on photosystem
483 I as well. We didn't measure any kinetic data for photosystem I, however; because of the
484 correlation between the kinetic data and photosystem II expression, our transcriptional
485 analysis provided some insight into the health of photosystem I. All 13 in-silica translated
486 transcripts from photosystem I, mapping to four *T. pseudonana* homologs, decreased in
487 abundance during UVR irradiation. One transcript, *psaB* which codes for photosystem I
488 P700 chlorophyll a apoprotein A2, had 6 variants with very similar abundance changes.
489 *PsaB* binds hydrophobically to *psaA* to form the major reaction center of photosystem I
490 (Falkowski and Raven 2007). The decreased abundance in *psaA*, a core reaction center
491 protein, likely indicates that the entire photosystem I reaction center complex was down-
492 regulated, correlating with the other photosystem I and II genes.
493 *Other Metabolic Pathway Expression*

494 UVR irradiation is known to cause other metabolic gene expression changes in
495 higher level plants (Jenkins 2009). We determined the gene expression changes for the
496 CBB cycle, the TCA cycle, and the glycolytic cycle. The glycolytic cycle is the first
497 phase in the catabolism of cellular carbohydrates (Nelson and Cox 2005). The TCA
498 cycle, the second phase of catabolism, is an important source of the cellular reducing
499 agent NADH, which helps generate the proton gradient that is critical for the production
500 of ATP through electron transport (Nelson and Cox 2005). Finally, the CBB cycle
501 performs carbon fixation for the cell, which provides the carbon skeletons necessary for
502 carbohydrate catabolism. In our study, glycolysis, the TCA cycle and the CBB cycle
503 produced a mixed gene expression pattern with many up and down regulated transcripts
504 directly after UVR irradiation. There are likely a variety of causative factors behind this
505 mixed pattern of expression including the susceptibility of certain enzymes to UV, as
506 well as direct transcriptomic regulation of certain enzymes which could in turn influence
507 the regulation of the entire pathway.
508 In plants, glycolytic regulation has been shown to often be dependent on the
509 tissue, as well as the external environment (Plaxton 1996). Phosphofructokinase,
510 important for fine control of glycolysis, mapped to two translated transcripts which
511 significantly decreased during UVR irradiation (Plaxton 1996). Phosphofructokinase is
512 the first committed step in the glycolysis pathway, and one of the major regulators of the
513 glycolytic pathway (Nelson and Cox 2005). The regulation of phosphofructokinase is so
514 important, in fact, that it can oftentimes overrule the regulatory roles of the other
515 glycolytic enzymes (Usenik and Legiša 2010). In fact, it has been observed that the
516 repression of a phosphofructokinase isoform can largely repress glycolysis and increase

517 the movement of glucose of through the pentose phosphate pathway, in order to increase
518 nucleotide production after UV induced DNA damage (Franklin et al. 2016). Like the
519 TCA cycle, the in-silica translated transcripts that mapped to homologs near the end of
520 the cycle (phosphoglycerate kinase – enolase), decreased in abundance after UVR
521 irradiation. Nonetheless, the slight majority of transcripts are increased directly after
522 UVR irradiation, possibly to try and keep a basal level of active glycolytic flux.
523 The TCA cycle also plays an important part in cellular respiration. In higher plant
524 species, such as *Arabidopsis thaliana*, previous research has shown UVR irradiation can
525 cause a mixed expression profile for the TCA pathway (Kusano et al. 2011; Cavalcanti et
526 al. 2014). Our data also illustrate a mixed expression pattern for the TCA cycle after
527 UVR irradiation. The first reaction in the TCA cycle, catalyzed by citrate synthase, was
528 strongly decreased during UVR irradiation with a single transcript variant. Moreover, it
529 was previously shown in plants that enzymes near the end of the TCA cycle reduced their
530 expression after UVR irradiation (Cavalcanti et al. 2014). For our experiment, the last
531 three enzymes in the cycle produced a mixed expression pattern.
532 Like TCA and glycolysis, the CBB cycle expression was mixed during UVR
533 irradiation. The CBB cycle is broken up into 3 main stages for the overall assimilation of
534 CO_2 fixation within the cell (Nelson and Cox 2005). The first stage is the fixation of CO_2
535 into 3-phosphoglycerate, which is catalyzed by the protein RuBisCO. RuBisCO is the
536 most abundant protein on Earth due the large amount needed by all plants for CO_2
537 fixation, and accounts for > 99.5% of inorganic carbon assimilated by primary producers
538 (Raven 2009; Raven 2013). Our data demonstrated a mixed expression pattern for the in-
539 silica translated transcripts mapping to the RuBisCO homolog, though the majority were

decreased in abundance compared to non-irradiated cells. Previous research on higher order plants demonstrated that UVR irradiation caused a large decrease in the activity and expression of RuBisCO when compared to control samples in pea leaves (Strid et al. 1990; Mackerness et al. 1999). Similar RuBisCO decreases were also observed in jackbeen leaves (Choi and Roh 2003).

The second stage of the CBB cycle involves the reduction of 3-phosphoglycerate to glyceraldehyde 3-phosphate (Nelson and Cox 2005). Expression for this stage was a mix of up-regulated and down-regulated transcripts, with the phosphoglycerate kinase homolog mapping to 2 translated transcripts that decreased in abundance, and the glyceraldehyde 3-phosphate homolog mapping to 1 translated transcript that decreased and 2 that increased in abundance.

The final stage of the CBB cycle involves the regeneration of RuBisCO. Several enzymes are responsible for this process, including sedoheptulose-bisphosphatase, which is an enzyme unique to the plastids. Sedoheptulose-bisphosphatase has no homolog in non-photosynthetic organisms, and likely plays a key role in the regulation of the carbon flux in the CBB cycle (Raines et al. 1999). There were 3 translated transcripts that mapped to the sedoheptulose-bisphosphatase homolog, all of them significantly increased in abundance over control levels (Supplementary Table S13). Possibly the cell is working to regenerate the available pools of RuBisCO, which were likely decreased due to UVR irradiation.

Preliminary Recovery

After 6 hours of recovery in dark conditions, several photosynthetic transcripts reversed their expression and displayed large increases in abundance compared to the

563 non-irradiated samples (Supplementary Table S14). This may indicate that the cell is
564 actively trying to repair certain aspects of its UV damaged photosynthetic clusters in
565 order to continue to survive. For example, transcripts that code for photosystem II psbV
566 and psbU proteins were part of the group that increased in abundance. These are extrinsic
567 proteins that help stabilize the photosystem II and the electron transfer (Roose et al.
568 2007). Both also have a large role in oxygen evolution, a major byproduct of the water
569 splitting reaction. As previously mentioned, the water splitting complex is a major target
570 of UVR irradiation (Post et al. 1996; Szilárd et al. 2007), thus possibly making it a
571 primary repair point. Homologous transcripts that were part of the cytochrome b6/f
572 complex or maintained roles in photosynthetic electron transport were also increased in
573 abundance after night recovery. The largest change in abundance was displayed by a PetF
574 transcript, which codes for the photosynthetic ferredoxin protein. In fact all of the
575 increased transcripts, which when translated map to cytochrome b6/f or photosynthetic
576 electron transport proteins, were part of the Pet family of genes. This may indicate that
577 the cells are trying to restart and repair electron transport before light begins to re-
578 energize the photosynthetic system. In summary, increased gene expression of may be a
579 cellular mechanism to restore the lost metabolic activity during UVR irradiation, a
580 necessary survival method.

581 Still, the majority of the photosystem I and II transcripts are significantly
582 decreased (Supplementary Table S14). In some cases UVR damage can be so
583 detrimental that certain species become more susceptible to permanent photosynthetic
584 damage, thus making the amount of recovery for the cell negligible (Neale et al. 1998;
585 Fritz et al. 2008). Our kinetic data support this notion as the photosynthetic efficiency and

586 turnover time of the organism are consistent for the first hour and a half, irrelevant of
587 energy intensity, as repair mechanisms mitigate the UVR induced damage (Fig. 2).
588 However, after an hour and a half at the highest intensities, and later at the lower
589 intensities, the repair system has possibly become overwhelmed and cannot keep up with
590 the increasing cell damage, thus there are large changes in electron transport rate and
591 turnover time. The absence of transcripts with increased abundance that map to
592 photosystem I and II genes may indicate that photosynthesis has become permanently
593 photoinhibited or *C. hystrix* has a very slow recovery rate. Different species employ
594 different repair mechanisms, and this may be a consequence of that (Bischof et al. 2006).
595 Metabolic recovery, based on the transcriptomic results, was evident as all three
596 of the pathways tested were strongly up-regulated after dark recovery (Fig. 4-6, S15-
597 S17). The median $\log_2$ fold change for every homolog of the three pathways was
598 significantly increased in abundance compared to the non-irradiated control, except for
599 the large subunit of RuBisCO. Taken as a whole, these results indicate a coordinated
600 transcriptomic response to up regulate necessary metabolic survival genes after intense
601 UVR irradiation. These metabolic enzymes provide the energy the cells need to duplicate
602 and survive, and indicate an active recovery response. Without these enzymes, the cell
603 will most certainly face a quick demise.
604
605 **Conclusions:**
606 Our custom emitter array produced morphological, physiological and molecular
607 responses with extremely high resolution and reproducibility. We demonstrate based on
608 *C. hystrix* physiological measurements, that with our emitter array we were able to

609 directly manipulate the speed and strength of photosynthetic damage based on the
610 specific applied UVR energy intensities. We can also induce metabolic expression
611 changes, which could change the entire metabolome of organisms. This ability to study
612 specific physiological and metabolic responses over a large spectrum of UVR intensities
613 could in the future provide further insights into UV induced damage and repair cycles in
614 other complex organisms. It also allows us to test many types of organisms under UV
615 stress conditions to identify those that are less susceptible to UV damage. These
616 organisms that are well adapted to high UV fluxes may contain novel mechanisms or
617 compounds that are used to alleviate damage, which could increase our understanding of
618 the diseases resulting from DNA damage.
619

620 **References:**

621 Allen AE, Laroche J, Maheswari U, Lommer M, Schauer N, Lopez PJ, Finazzi G, Fernie
622 AR, Bowler C (2008) Whole-cell response of the pennate diatom *Phaeodactylum*
623 *tricornutum* to iron starvation. Proc Natl Acad Sci U S A 105:10438–10443. doi:
624 10.1073/pnas.0711370105

625 Allen AE, Vardi A, Bowler C (2006) An ecological and evolutionary context for
626 integrated nitrogen metabolism and related signaling pathways in marine diatoms.
627 Current Opinion in Plant Biology 9:264–273. doi: 10.1016/j.pbi.2006.03.013

628 Andrews S (2009) FastQC A Quality Control tool for High Throughput Sequence Data.

629 Armbrust EV (2009) The life of diatoms in the world's oceans. Nat Geosci 459:185–92.

630 Bender SJ, Durkin CA, Berthiaume CT, Morales RL, Armbrust EV (2014)
631 Transcriptional responses of three model diatoms to nitrate limitation of growth.
632 Front Mar Sci 1:3. doi: 10.3389/fmars.2014.00003

633 Berardesca E, Bertona M, Altabas K, Altabas V, Emanuele E (2012) Reduced ultraviolet-
634 induced DNA damage and apoptosis in human skin with topical application of a
635 photolyase-containing DNA repair enzyme cream: clues to skin cancer prevention.
636 Mol Med Rep 5:570–574. doi: 10.3892/mmr.2011.673

637 Bischof K, Gómez I, Molis M, Hanelt D, Karsten U, Lüder U, Roleda MY, Zacher K,
638 Wiencke C (2006) Ultraviolet radiation shapes seaweed communities. Rev Environ
639 Sci Biotechnol 5:141–166. doi: 10.1007/s11157-006-0002-3

640 Bolger AM, Lohse M, Usadel B (2014) Trimmomatic: a flexible trimmer for Illumina
641 sequence data. Bioinformatics 30:2114–2120. doi: 10.1093/bioinformatics/btu170

642 Bornman JF, Vogelmann TC (1991) Effect of UV-B Radiation on Leaf Optical Properties
643 Measured with Fibre Optics. J Exp Bot 42:547–554.

644 Bouchard JN, Roy S, Campbell DA (2006) UVR Effects on the Photosystem II-D1
645 Protein of Phytoplankton and Natural Phytoplankton Communities. Photochemistry
646 and Photobiology 82:936–17. doi: 10.1562/2005-08-31-IR-666

647 Cavalcanti JHF, Esteves-Ferreira AA, Quinhones CGS, Pereira-Lima IA, Nunes-Nesi A,
648 Fernie AR, Araújo WL (2014) Evolution and functional implications of the
649 tricarboxylic acid cycle as revealed by phylogenetic analysis. Genome Biol Evol
650 6:2830–2848. doi: 10.1093/gbe/evu221

651 Choi BY, Roh KS (2003) UV-B Radiation Affects Chlorophyll and Activation of
652 Rubisco by Rubisco Activase in *Canavalia ensiformis* L. Leaves. Journal of Plant
653 Biology 46:117–121. doi: 10.1007/BF03030440

654 Coesel S, Mangogna M, Ishikawa T, Heijde M, Rogato A, Finazzi G, Todo T, Bowler C,

655 Falciatore A (2009) Diatom PtCPF1 is a new cryptochrome/photolyase family
656 member with DNA repair and transcription regulation activity. EMBO reports
657 10:655–661. doi: 10.1038/embor.2009.59

658 Critchley C (2000) Photoinhibition. In: Raghavendra AS (ed) Photosynthesis A
659 Comprehensive Treatise. Cambridge, UK, pp 264–272

660 Cullen JJ, Lesser MP (1991) Inhibition of photosynthesis by ultraviolet radiation as a
661 function of dose and dosage rate: Results for a marine diatom. Mar Biol 111:183–
662 190. doi: 10.1007/BF01319699

663 Domingues N, Matos AR, Marques da Silva J, Cartaxana P (2012) Response of the
664 Diatom *Phaeodactylum tricornutum* to Photooxidative Stress Resulting from High
665 Light Exposure. PLoS ONE 7:e38162–6. doi: 10.1371/journal.pone.0038162

666 Dyhrman ST, Jenkins BD, Rynearson TA, Saito MA, Mercier ML, Alexander H,
667 Whitney LP, Drzewianowski A, Bulygin VV, Bertrand EM, Wu Z, Benitez-Nelson
668 C, Heithoff A (2012) The transcriptome and proteome of the diatom *Thalassiosira*
669 *pseudonana* reveal a diverse phosphorus stress response. PLoS ONE 7:e33768. doi:
670 10.1371/journal.pone.0033768

671 Emanuele E, Altabas V, Altabas K, Berardesca E (2013) Topical application of
672 preparations containing DNA repair enzymes prevents ultraviolet-induced telomere
673 shortening and c-FOS proto-oncogene hyperexpression in human skin: an
674 experimental pilot study. J Drugs Dermatol 12:1017–1021.

675 Falkowski PG, Raven JA (2007) Aquatic Photosynthesis, 2nd edn. Princeton

676 Franklin DA, He Y, Leslie PL, Tikunov AP, Fenger N, Macdonald JM, Zhang Y (2016)
677 p53 coordinates DNA repair with nucleotide synthesis by suppressing PFKFB3
678 expression and promoting the pentose phosphate pathway. Sci Rep 6:1–13. doi:
679 10.1038/srep38067

680 Fritz JJ, Neale PJ, Davis RF, Peloquin JA (2008) Response of Antarctic phytoplankton to
681 solar UVR exposure: inhibition and recovery of photosynthesis in coastal and pelagic
682 assemblages. Marine Ecology Progress Series 365:1–16. doi: 10.3354/meps07610

683 Geider RJ, Greene RM, Kolber Z, MacIntyre HL, Falkowski PG (1993) Fluorescence
684 assessment of the maximum quantum efficiency of photosynthesis in the western
685 North Atlantic. Deep-Sea Res Pt I 40:1205–1224. doi: 10.1016/0967-0637(93)90134-
686 o

687 Gilstad M, Sakshaug E (1990) Growth rates of ten diatom species from the Barents Sea at
688 different irradiances and day lengths. Marine Ecology Progress Series 64:169–173.
689 doi: 10.3354/meps064169

690 Gladman S, Seemann T **VelvetOptimiser**

691 .

692 Greenberg B, Wilson M, Huang X-D, Duxbury C, Gerhardt K, Gensemer R (1997) The
693 effects of ultraviolet-B radiation on higher plants. In: Plants for Environmental
694 Studies. CRC Press, pp 1–35

695 Guillard RRL, Hargraves PE (1993) *Stichochrysis immobilis* is a diatom, not a
696 chrysophyte. Phycologia 32:234–236.

697 Helbling EW, Chalker BE, Dunlap WC, Holm-Hansen O, Villafane VE (1996)
698 Photoacclimation of Antarctic marine diatoms to solar ultraviolet radiation. Journal
699 of Experimental Marine Biology and Ecology 204:85–101. doi: 10.1016/0022-
700 0981(96)02591-9

701 Herbstová M, Bína D, Koník P, Gardian Z, Vácha F, Litvín R (2015) Molecular basis of
702 chromatic adaptation in pennate diatom *Phaeodactylum tricornutum*. BBA-
703 Bioenergetics 1847:534–543. doi: 10.1016/j.bbabio.2015.02.016

704 Huang L, McCluskey MP, Ni H, LaRossa RA (2002) Global Gene Expression Profiles of
705 the Cyanobacterium *Synechocystis* sp. Strain PCC 6803 in Response to Irradiation
706 with UV-B and White Light. J Bacteriol 184:6845–6858. doi:
707 10.1128/JB.184.24.6845-6858.2002

708 Jenkins GI (2009) Signal Transduction in Responses to UV-B Radiation. Annu Rev Plant
709 Biol 60:407–431. doi: 10.1146/annurev.arplant.59.032607.092953

710 Kanehisa M, Goto S (2000) KEGG: kyoto encyclopedia of genes and genomes. Nucleic
711 Acids Res 28:27–30.

712 Kanehisa M, Goto S, Sato Y, Kawashima M, Furumichi M, Tanabe M (2013) Data,
713 information, knowledge and principle: back to metabolism in KEGG. Nucleic Acids
714 Res 42:D199–D205. doi: 10.1093/nar/gkt1076

715 Kolber Z, Falkowski PG (1993) Use of active fluorescence to estimate phytoplankton
716 photosynthesis in situ. Limnol Oceanogr 38:1646–1665. doi:
717 10.4319/lo.1993.38.8.1646

718 Kolber Z, Zehr J, Falkowski P (1988) Effects of Growth Irradiance and Nitrogen
719 Limitation on Photosynthetic Energy Conversion in Photosystem II. Plant Physiol
720 88:923–929.

721 Kolber ZS, Prášil O, Falkowski PG (1998) Measurements of variable chlorophyll
722 fluorescence using fast repetition rate techniques: defining methodology and
723 experimental protocols. BBA 1367:88–106. doi: 10.1016/s0005-2728(98)00135-2

724 Kusano M, Tohge T, Fukushima A, Kobayashi M, Hayashi N, Otsuki H, Kondou Y,
725 Goto H, Kawashima M, Matsuda F, Niida R, Matsui M, Saito K, Fernie AR (2011)
726 Metabolomics reveals comprehensive reprogramming involving two independent

727 metabolic responses of Arabidopsis to UV-B light. The Plant Journal 67:354–369.
728 doi: 10.1111/j.1365-313X.2011.04599.x

729 Langmead B, Salzberg SL (2012) Fast gapped-read alignment with Bowtie 2. Nat
730 Methods 9:357–359. doi: 10.1038/nmeth.1923

731 Ligowski R, Jordan RW, Assmy P (2012) Morphological adaptation of a planktonic
732 diatom to growth in Antarctic sea ice. Mar Biol 159:817–827. doi: 10.1007/s00227-
733 011-1857-6

734 Lohman KE (1960) The Ubiquitous Diatom–A Brief Survey Of The Present State Of
735 Knowledge. Am J Sci A 258:180–191.

736 Love MI, Huber W, Anders S (2014) Moderated estimation of fold change and dispersion
737 for RNA-seq data with DESeq2. Genome Biol 15:550. doi: 10.1186/s13059-014-
738 0550-8

739 Mackerness S, Jordan BR, Thomas B (1999) Reactive oxygen species in the regulation of
740 photosynthetic genes by ultraviolet-B radiation (UV-B: 280–320 nm) in green and
741 etiolated buds of pea (*Pisum sativum* L.). J Photochem Photobiol B: Biol 48:180–
742 188. doi: 10.1016/s1011-1344(99)00024-x

743 Marchetti A, Schruth DM, Durkin CA, Parker MS, Kodner RB, Berthiaume CT, Morales
744 R, Allen AE, Armbrust EV (2012) Comparative metatranscriptomics identifies
745 molecular bases for the physiological responses of phytoplankton to varying iron
746 availability. Proc Natl Acad Sci U S A 109:E317–25. doi: 10.1073/pnas.1118408109

747 Mauzerall D (1986) The optical cross section and absolute size of a photosynthetic unit.
748 Photosynth Res 10:163–170. doi: 10.1007/BF00118279

749 Melis A, Nemson JA, Harrison MA (1992) Damage to functional components and partial
750 degradation of photosystem II reaction center proteins upon chloroplast exposure to
751 ultraviolet-B radiation. BBA-Bioenergetics 1100:312–320. doi: 10.1016/0167-
752 4838(92)90487-x

753 Neale PJ, Cullen JJ, Davis RF (1998) Inhibition of marine photosynthesis by ultraviolet
754 radiation: Variable sensitivity of phytoplankton in the Weddell-Scotia Confluence
755 during the austral spring. Limnol and Oceanogr 43:433–448. doi:
756 10.4319/lo.1998.43.3.0433

757 Nelson DL, Cox MM (2005) Lehninger Principles of Biochemistry, 4 edn. W. H.
758 Freeman and Company

759 Norton TA, Melkonian M, Andersen RA (1996) Algal biodiversity. Phycologia 35:308–
760 326. doi: 10.2216/i0031-8884-35-4-308.1

761 Oxborough K, Moore CM, Suggett DJ, Lawson T, Chan HG, Geider RJ (2012) Direct
762 estimation of functional PSII reaction center concentration and PSII electron flux on

763 a volume basis: a new approach to the analysis of Fast Repetition Rate fluorometry
764 (FRRf) data. Limnol Oceanogr Met 10:142–154. doi: 10.4319/lom.2012.10.142

765 Pierre Y, Breyton C, Kramer D, Popot JL (1995) Purification and characterization of the
766 cytochrome b6 f complex from Chlamydomonas reinhardtii. J Biol Chem
767 270:29342–29349.

768 Plaxton WC (1996) THE ORGANIZATION AND REGULATION OF PLANT
769 GLYCOLYSIS. Annu Rev Plant Physiol Plant Mol Biol 47:185–214. doi:
770 10.1146/annurev.arplant.47.1.185

771 Post A, Lukins PB, Walker PJ, Larkum AW (1996) The effects of ultraviolet irradiation
772 on $P680^{+}$ reduction in PS II core complexes measured for individual S-states and
773 during repetitive cycling of the oxygen-evolving complex. Photosynth Res 49:21–27.
774 doi: 10.1007/BF00029424

775 Prestegard SK, Oftedal L, Coyne RT, Nygaard G, Skjærven KH, Knutsen G, Døskeland
776 SO, Herfindal L (2009) Marine Benthic Diatoms Contain Compounds Able to Induce
777 Leukemia Cell Death and Modulate Blood Platelet Activity. Mar Drugs 7:605–623.
778 doi: 10.3390/md7040605

779 Ragni M, Airs RL, Leonardos N, Geider RJ (2008) Photoinhibition of PsII in *Emiliania*
780 *Huxleyi* (Haptophyta) Under High Light Stress: the Roles of Photoacclimation,
781 Photoprotection, and Photorepair. J Phycol 44:670–683. doi: 10.1111/j.1529-
782 8817.2008.00524.x

783 Raines CA, Lloyd JC, Dyer TA (1999) New insights into the structure and function of
784 sedoheptulose-1,7-bisphosphatase; an important but neglected Calvin cycle enzyme.
785 J Exp Bot 50:1–8. doi: 10.1093/jxb/50.330.1

786 Rajagopal S, Murthy SD, Mohanty P (2000) Effect of ultraviolet-B radiation on intact
787 cells of the cyanobacterium *Spirulina platensis*: characterization of the alterations in
788 the thylakoid membranes. J Photochem Photobiol B: Biol 54:61–66. doi:
789 10.1016/S1011-1344(99)00156-6

790 Raven JA (2009) Contributions of anoxygenic and oxygenic phototrophy and
791 chemolithotrophy to carbon and oxygen fluxes in aquatic environments. Aquat
792 Microb Ecol 56:177–192. doi: 10.3354/ame01315

793 Raven JA (2013) Rubisco: still the most abundant protein of Earth? New Phytol 198:1–3.
794 doi: 10.1111/nph.12197

795 Remmert M, Biegert A, Hauser A, Söding J (2012) HHblits: lightning-fast iterative
796 protein sequence searching by HMM-HMM alignment. Nat Methods 9:173–175. doi:
797 10.1038/nmeth.1818

798 Roberts A, Pachter L (2012) Streaming fragment assignment for real-time analysis of
799 sequencing experiments. Nat Methods 10:71–73. doi: 10.1038/nmeth.2251

800 Roose JL, Wegener KM, Pakrasi HB (2007) The extrinsic proteins of Photosystem II.
801 Photosynth Res 92:369–387. doi: 10.1007/s11120-006-9117-1

802 Schulz MH, Zerbino DR, Vingron M, Birney E (2012) Oases: robust de novo RNA-seq
803 assembly across the dynamic range of expression levels. Bioinformatics 28:1086–
804 1092. doi: 10.1093/bioinformatics/bts094

805 Sharon Y, Dishon G, Beer S (2011) The Effects of UV Radiation on Chloroplast
806 Clumping and Photosynthesis in the Seagrass *Halophila stipulacea* Grown under
807 High-PAR Conditions. Journal of Marine Biology 2011:1–6. doi:
808 10.1155/2011/483428

809 Shrestha RP, Tesson B, Norden-Krichmar T, Federowicz S, Hildebrand M, Allen AE
810 (2012) Whole transcriptome analysis of the silicon response of the diatom
811 *Thalassiosira pseudonana*. BMC Genomics 13:499. doi: 10.1186/1471-2164-13-499

812 Soding J (2005) Protein homology detection by HMM-HMM comparison. Bioinformatics
813 21:951–960. doi: 10.1093/bioinformatics/bti125

814 Strid Å, Chow WS, Anderson JM (1990) Effects of supplementary ultraviolet-B radiation
815 on photosynthesis in *Pisum sativum*. BBA 1020:260–268. doi: 10.1016/0005-
816 2728(90)90156-x

817 Suggett DJ, Moore CM, Hickman AE, Geider RJ (2009) Interpretation of fast repetition
818 rate (FRR) fluorescence: signatures of phytoplankton community structure versus
819 physiological state. Marine Ecology Progress Series 376:1–19. doi:
820 10.3354/meps07830

821 Surplus SL, Jordan BR, Murphy AM, Carr JP, Thomas B, Mackerness SAH (1998)
822 Ultraviolet-B-induced responses in *Arabidopsis thaliana*: role of salicylic acid and
823 reactive oxygen species in the regulation of transcripts encoding photosynthetic and
824 acidic pathogenesis-related proteins. Plant, Cell and Environment 21:685–694. doi:
825 10.1046/j.1365-3040.1998.00325.x

826 Szilárd A, Sass L, Deák Z, Vass I (2007) The sensitivity of Photosystem II to damage by
827 UV-B radiation depends on the oxidation state of the water-splitting complex. BBA
828 1767:876–882. doi: 10.1016/j.bbabio.2006.11.020

829 Teramura AH, Ziska LH (1996) Ultraviolet-B Radiation and Photosynthesis. In:
830 Photosynthesis and the Environment. Springer Netherlands, Dordrecht, pp 435–450

831 Usenik A, Legiša M (2010) Evolution of allosteric citrate binding sites on 6-
832 phosphofructo-1-kinase. PLoS ONE 5:e15447. doi: 10.1371/journal.pone.0015447

833 Vass I, Sass L, Spetea C, Bakou A, Ghanotakis DF, Petrouleas V (1996) UV-B-induced
834 inhibition of photosystem II electron transport studied by EPR and chlorophyll
835 fluorescence. Impairment of donor and acceptor side components. Biochemistry
836 35:8964–8973. doi: 10.1021/bi9530595

837 Verde C, Prisco GD (2012) Adaptation and Evolution in Marine Environments, Volume
838 2: The Impacts of Global Change on Biodiversity. Springer, Berlin/Heidelberg

839 Vincent WF (1988) Microbial ecosystems of Antarctica. Cambridge University Press

840 Wickham H (2009) ggplot2: elegant graphics for data analysis. Springer New York

841 Wu Y, Li Z, Du W, Gao K (2015) Physiological response of marine centric diatoms to
842 ultraviolet radiation, with special reference to cell size. J Photochem Photobiol B:
843 Biol 153:1–6. doi: 10.1016/j.jphotobiol.2015.08.035

844 Zerbino DR, Birney E (2008) Velvet: Algorithms for de novo short read assembly using
845 de Bruijn graphs. Genome Res 18:821–829. doi: 10.1101/gr.074492.107

846 Zhang Z-S, Jin L-Q, Li Y-T, Tikkanen M, Li Q-M, Ai X-Z, Gao H-Y (2016) Ultraviolet-
847 B Radiation (UV-B) Relieves Chilling-Light-Induced PSI Photoinhibition And
848 Accelerates The Recovery Of CO2 Assimilation In Cucumber (Cucumis sativus L.)
849 Leaves. Sci Rep 1–10. doi: 10.1038/srep34455

850

851

852 **Figure Legends**

853 Figure 1: Schematic of custom built UVR emitter array. The numbers in the legend to the
854 left of the diagram correspond to the specific component of our setup.

855

856 Figure 2: **A:** Fv/Fm as a measure of the maximum quantum yield of PSII. **B:** Sigma as a
857 proxy for functional cross section and effective target size of the PSII antenna in $Å^2$
858 $(quanta)^{-1}$. **C**: Tau 1 turnover time. During every hour at 0.32 mW/cm^2 and 0.64 mW/cm^2,
859 and every half hour at 0.96-1.59 mW/cm^2 the tau 1 turnover time was calculated using
860 Fast Repetition Rate Fluorometry (FRRF). Irradiation time is on the x-axis with the
861 turnover time in µs on the y-axis. **D**: Tau 2 turnover time. During every hour at 0.32
862 mW/cm^2 and 0.64 mW/cm^2, and every half hour at 0.96-1.59 mW/cm^2 the tau 2 turnover
863 time was calculated using Fast Repetition Rate Fluorometry (FRRF). Irradiation time is
864 on the x-axis with the turnover time in µs on the y-axis. Note the drop in turnover time at
865 1.28 and 1.59 mW/cm^2.

866

867 Figure 3: Box and whisker plot for *T. pseudonana* photosynthetic homologs. Log_2 fold
868 changes directly after UVR irradiation are represented in the left figure – labeled "Day" –
869 while log_2 fold changes after six-hour dark recovery – labeled "Night" – are represented
870 in the figure to the right. The line within the box is the median of the log_2 fold changes
871 for that specific homolog. The hinges are the 1st and 3rd quartile. The upper whisker starts
872 from the hinge and ends at the highest value that is within 1.5 * inter-quartile range of the
873 hinge. The lower whisker extends form the hinge to the lowest value that is within 1.5 *
874 inter-quartile range. The x-axis is consistent between both figures, therefore some

875 homologs (e.g. cytochrome c6 – directly after UVR irradiation; photosystem II CP47 –
876 after dark recovery) will have missing data in their specific figure, as there were no
877 differentially expressed translated transcripts mapping to that homolog during that time.
878
879 Figure 4: Box and whisker plot for *T. pseudonana* glycolysis homologs. Log_2 fold
880 changes directly after UVR irradiation are represented in the left figure – labeled "Day" –
881 while log_2 fold changes after six-hour dark recovery – labeled "Night" – are represented
882 in the figure to the right. The line within the box is the median of the log_2 fold changes
883 for that specific homolog. The hinges are the 1st and 3rd quartile. The upper whisker starts
884 from the hinge and ends at the highest value that is within 1.5 * inter-quartile range of the
885 hinge. The lower whisker extends form the hinge to the lowest value that is within 1.5 *
886 inter-quartile range. The x-axis is consistent between both figures, therefore some
887 homologs (e.g. phosphoglucomutase – directly after UVR irradiation) will have missing
888 data in their specific figure, as there were no differentially expressed translated
889 transcripts mapping to that homolog during that time.
890
891 Figure 5: Box and whisker plot for *T. pseudonana* TCA homologs. Log_2 fold changes
892 directly after UVR irradiation are represented in the left figure – labeled "Day" – while
893 log_2 fold changes after six-hour dark recovery – labeled "Night" – are represented in the
894 figure to the right. The line within the box is the median of the log_2 fold changes for that
895 specific homolog. The hinges are the 1st and 3rd quartile. The upper whisker starts from
896 the hinge and ends at the highest value that is within 1.5 * inter-quartile range of the
897 hinge. The lower whisker extends form the hinge to the lowest value that is within 1.5 *

898 inter-quartile range. The x-axis is consistent between both figures, therefore some
899 homologs (e.g. 2-oxoglutarate dehydrogenase E1 – directly after UVR irradiation) will
900 have missing data in their specific figure, as there were no differentially expressed
901 translated transcripts mapping to that homolog during that time.
902
903 Figure 6: Box and whisker plot for *T. pseudonana* CBB Cycle homologs. Log_2 fold
904 changes directly after UVR irradiation are represented in the left figure – labeled "Day" –
905 while log_2 fold changes after six-hour dark recovery – labeled "Night" – are represented
906 in the figure to the right. The line within the box is the median of the log_2 fold changes
907 for that specific homolog. The hinges are the 1st and 3rd quartile. The upper whisker starts
908 from the hinge and ends at the highest value that is within 1.5 * inter-quartile range of the
909 hinge. The lower whisker extends form the hinge to the lowest value that is within 1.5 *
910 inter-quartile range. The x-axis is consistent between both figures, therefore some
911 homologs (e.g. ribose 5-phosphate isomerase A – directly after UVR irradiation) will
912 have missing data in their specific figure, as there were no differentially expressed
913 translated transcripts mapping to that homolog during that time.
914

Figure #1.

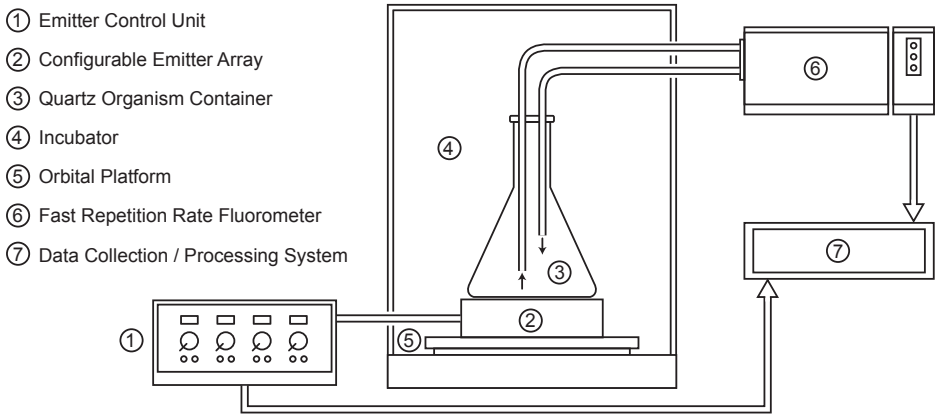

Figure #2.

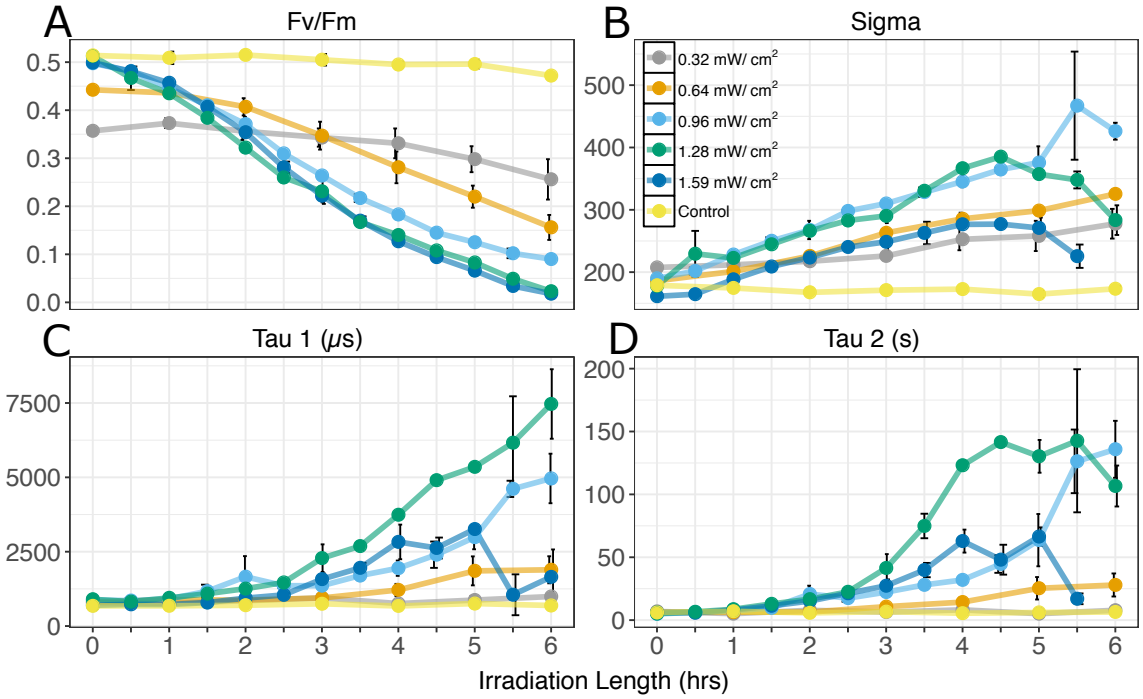

Figure #3.

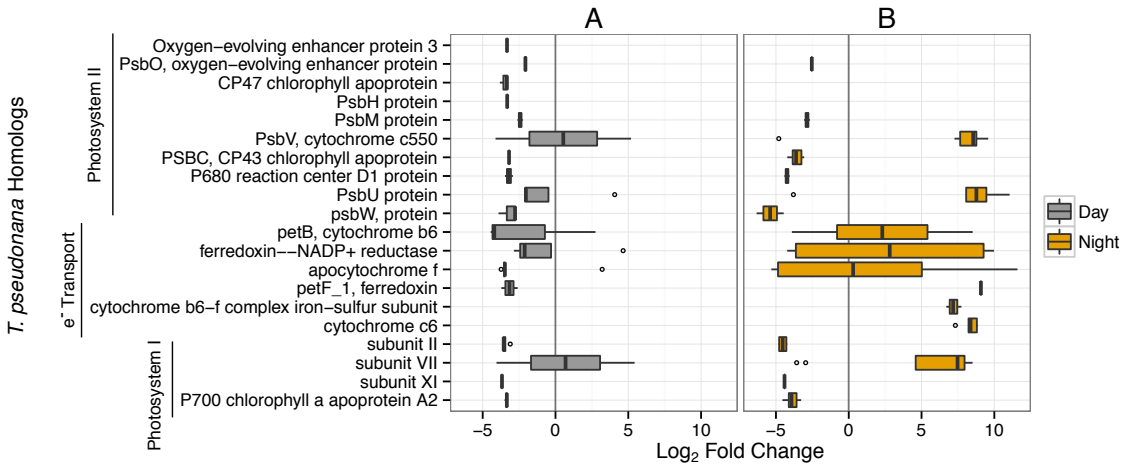

Figure #4.

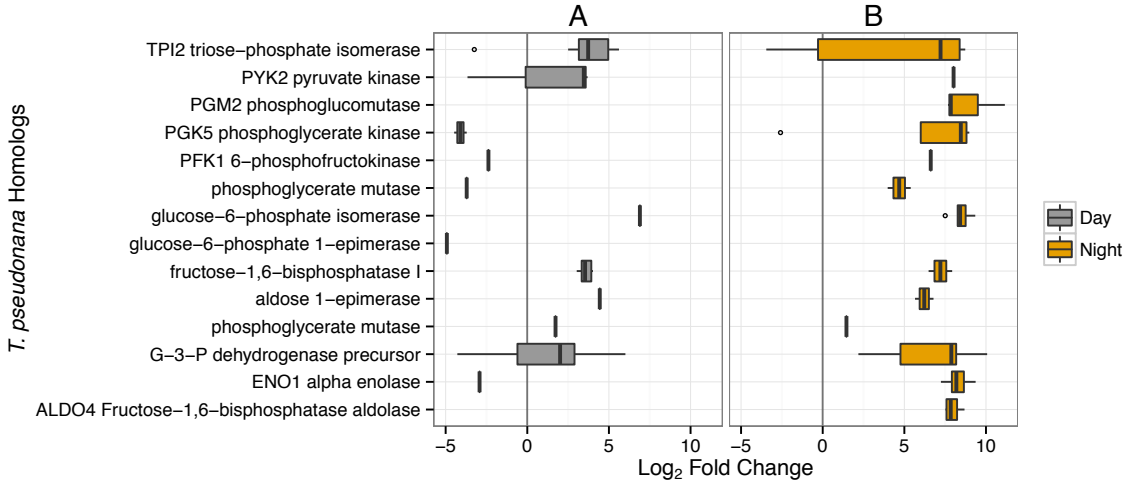

Figure #5.

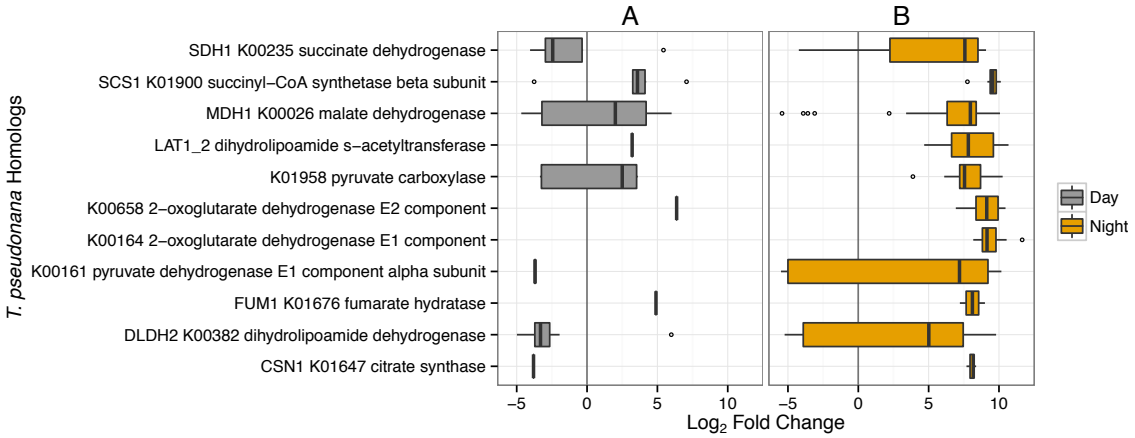

Figure #6.